atmosphere

MDPI

Article

Aerosol Optical Properties and Contribution to Differentiate Haze and Haze-Free Weather in Wuhan City

Miao Zhang [1], Jing Liu [2], Muhammad Bilal [3,*], Chun Zhang [1], Majid Nazeer [4], Luqman Atique [5], Ge Han [6] and Wei Gong [7]

1 School of Environmental Science and Tourism, Nanyang Normal University, Wolong Road No. 1638, Nan Yang 473061, China; zm_liesmars@whu.edu.cn (M.Z.); zchun0192@nynu.edu.cn (C.Z.)
2 Lingnan College, Sun Yat-sen University, Guangzhou 510275, China; liuj243@mail2.sysu.edu.cn
3 School of Marine Sciences, Nanjing University of Information Science & Technology, Nanjing 2100444, China
4 Key Laboratory of Digital Land and Resources, East China University of Technology, Nanchang 330013, China; majidnazeer@ecit.cn
5 School of Earth Sciences, Zhejiang University, Hangzhou 310027, China; lagondal@zju.edu.cn
6 School of Remote Sensing and Information Engineering, Wuhan University, Luoyu Road No. 129, Wuhan 430079, China; udhan@whu.edu.cn
7 State Key Laboratory of Information Engineering in Surveying, Mapping and Remote Sensing, Wuhan University, Wuhan 430079, China; weigong@whu.edu.cn
* Correspondence: muhammad.bilal@connect.polyu.hk; Tel.: +86-132-6085-6312

Received: 2 March 2020; Accepted: 25 March 2020; Published: 27 March 2020

Abstract: Haze is an atmospheric phenomenon in which different types of particulates obscure the sky, and hence affect almost all human activities. Over a couple of recent decades, China has witnessed increasingly worse air quality as well as atmospheric haziness in its cities. There are various haze contributing factors including the rapid industrialization, excessive biomass burning, and an increase in the number of vehicles. This study proposes a methodology based on the aerosols scattering and absorption properties, to predict the likelihood of an episode of hazy days. This case study employs the aerosol optical properties data from integrated nephelometer and aethalometer sensors from December 2009 to September 2014 over Wuhan. The role and contribution of each aerosol optical parameter (e.g., aerosol scattering and absorption coefficients, single scattering albedo, scattering, and absorption Ångström exponents, backscatter ratio, and asymmetry factor) in distinguishing haze and haze-free conditions has been quantitatively determined based on a machine learning approach. Each aerosol optical parameter was classified independently by the support vector machine (SVM) algorithm, and the aerosol scattering (85.37%) and absorption (74.53%) coefficients were found to be primary potential indicators. Through the Kolmogorov-Smirnov test and traditional statistical analysis, the aerosol scattering and absorption coefficients were then verified as important indicators in distinguishing haze and haze-free days. Finally, through a probability density diagram and frequency histogram, we propose a simple quantitative standard to distinguish between haze and haze-free conditions based on the aerosol scattering coefficient and absorption coefficient in Wuhan City. The accuracy of the standard was determined to be 81.49% after testing, which indicates an accurate result. An error in aerosol optical properties may lead to an error in the calculation of aerosol radiative forcing, the earth's energy budget, and climate prediction. Therefore, understanding of the aerosol properties during haze-free and haze-days will help policymakers to make new policies to control urban pollution and their effects on human health.

Keywords: aerosols; atmospheric scattering; absorption; atmospheric haze; machine learning

1. Introduction

Aerosols are microscopic solid particles or droplets in the atmosphere [1–6], and the World Health Organization has defined that particles with diameters smaller than 2.5 microns ($PM_{2.5}$) can enter human blood circulation systems, causing vascular inflammation and atherosclerosis [7,8]. The Intergovernmental Panel on Climate Change (IPCC) stated that aerosols are one of the leading uncertain factors that induce the climate change, as aerosols can directly affect the earth's radiation balance by scattering and absorbing solar short-wave radiation and thermal infrared long-wave radiation, and the changes in cloud nuclei aerosols can control cloud's physical properties and life cycle, which can indirectly affect the earth's climate system [9–11].

In China, which has experienced rapid economic development in recent years, increased industrial and urbanization activities have led to an increased number of aerosol particles, and, in turn, enhanced air pollution events [12]. At present, the definition of haze standards is not consistent around the world. For example, the Chinese Meteorological Administration (CMA) decided that if visibility value is less than 10 km and relative humidity (RH) is less than 95%, it is haze weather. However, in some studies, researchers reported that if visibility values are less than 5 km and RH values are less than 80%, it defines haze weather [13,14]. In recent past, impactful regional scale haze events have occurred in the Pearl River Delta (PRD) [15], Yangtze River Delta (YRD) [16], the Beijing-Tianjin-Hebei urban agglomeration (BTH) [17,18], and semi-arid northwestern areas of the country [19]. Different types of haze (dust, brown smoke, black carbon) have variable impacts on the regional and global climate [20]. Haze from soot particles can be an absorbent and act to heat the atmosphere, cooling the earth's surface [21]. Studies of haze have also attracted the attention of many researchers in recent years. These studies aimed to explore the causes, optical and physical properties, and chemical compositions of the haze-causing aerosols. Similar studies have also found that haze aerosol particles have positive heating effects on atmospheric fluxes [20,22], and serious haze events have been closely related to certain meteorological conditions and anthropogenic pollutant emissions [23,24].

Various researches have reported that aerosol optical parameters can quantitatively reflect aerosol radiation forcing, especially on haze days [10,11,25]. These optical parameters have been widely investigated on haze and haze-free days, but their ability to distinguish between weather types is still unknown and has not been studied previously [13]. Also, the classification of different aerosol categories has been the first step in retrieving aerosol optical properties in some projects, such as the Cloud-Aerosol LiDAR and Infrared Pathfinder Satellite Observation (CALIPSO) and Lidar In-Space Technology Experiment (LITE) programs [26,27]. However, no explicit criteria exist to distinguish between haze and haze-free aerosols yet. The differences in the aerosol optical properties between these two weather types (i.e., hazy and clear sky) can lead to a more detailed understanding of the haze radiative effect. For example, we can identify which parameter changes significantly from haze-free to hazy days, while providing a convenient and simple criterion to classify haze and haze-free aerosols and assist in the retrieval of aerosol optical properties. At present, visibility is the basic index to define haze-causing aerosols [14]; therefore, a comprehensive defining criterion based on optical parameters for haze is necessary.

The aim of this study, first, is to investigate the optical and physical properties of aerosols in Wuhan. Second, it further explores the contribution of each optical and physical parameter of haze and haze-free aerosols. Finally, according to the optical parameters with large contributions (weights), a convenient and simple optical criterion is proposed to distinguish haze from haze-free aerosols, to help us better understand the radiation forcing effect of haze aerosols. To our knowledge, there is no such study available before. The following section of this paper presents the experimental methodology, including data sources and study area. The third section details the results and discussion. Finally, the fourth part summarizes the conclusion.

2. Experimental Methodology

2.1. Study Area, Equipment and Data

Our experimental site is in the Wuhan University (29.97 degrees north latitude, 113.91 degrees east longitude) (Figure 1). Wuhan city is the capital of Hubei province and it is a mega inland city in central China, which is at the confluence of the Yangtze and Han rivers. The climate type of Wuhan is subtropical monsoon climate: winter is cold, summer is hot, humidity is high in summer and the annual precipitation is high. The aerosols mainly originate from traffic emission, industrial pollutants emission, fossil fuel combustion, and straw combustion, etc., [2,3]. Our research was conducted at the State Key Laboratory of Surveying, Mapping, and Remote Sensing Information Engineering (LISMARS), Wuhan University. The aerosol optical characteristics were principally obtained from nephelometer and aethalometer. The observation equipment was settled on the top of the laboratory [3]. The laboratory is close to a bustling highway, and the surrounding environment has industrial, commercial, and residential areas.

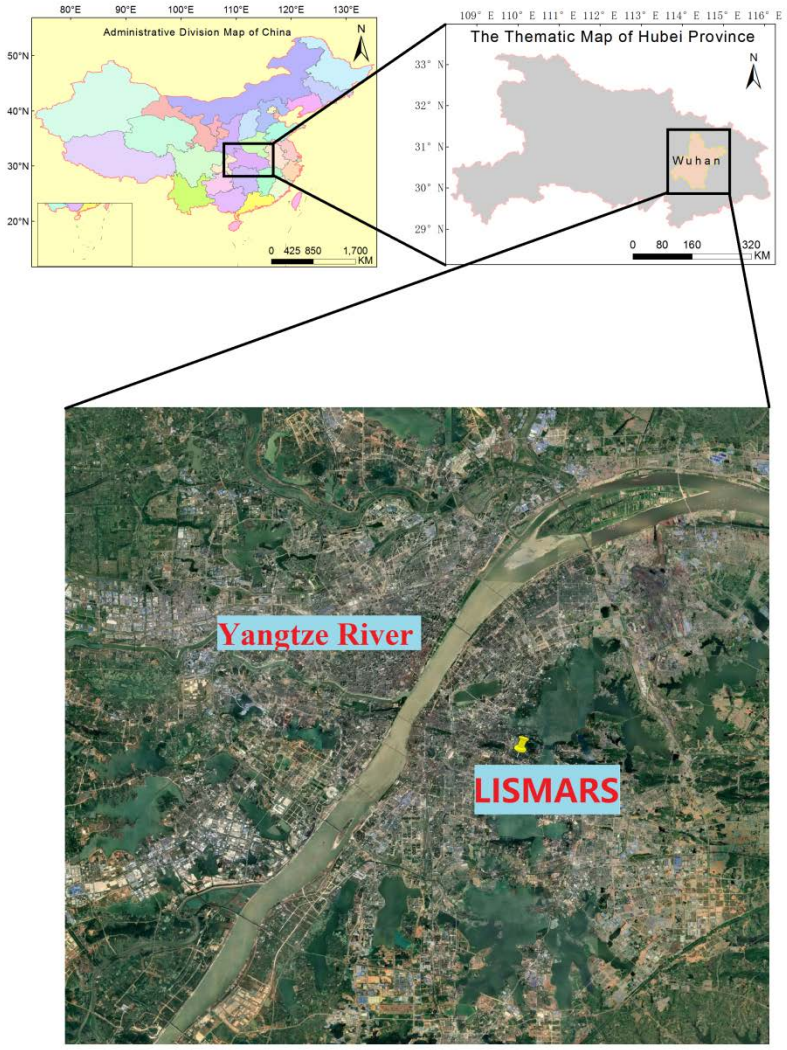

Figure 1. The experiment location of the observation site.

We collected datasets of aerosol optical parameters for 370 haze-free days and 662 haze days from December 2009 to September 2014. The working bands of the nephelometer were 450 nm, 550 nm, and 700 nm, and it can directly provide aerosol scattering coefficients and backscattering coefficients. The instrument operated automatically every day, and we use standard CO_2 to collaborate it every

three months [28,29]. The constituents of the outside environment and atmosphere were pumped in the equipment main cavity through a 3-m stainless steel pipe. The flow rate of the nephelometer was 30 L·min^{-1} and the sampling frequency was 1 min. The aerosol scattering properties could be measured at 7°–170° angle [30]. At the same time, the truncation error increases when there are large aerosol particles (such as dust) and we also conducted the truncation error correction before further processing of the dataset. The detection limit values of the scattering coefficient at their band were 0.44, 0.17, and 0.26 Mm^{-1}, respectively. The detection limit values of backscattering coefficient were 0.29, 0.11, and 0.21 mm^{-1}, respectively [30]. Data values beyond the limit were excluded from the calculation.

The aethalometer worked on seven wavelengths: 370, 470, 520, 590, 660, 880, and 950 nm. The 880 nm was the pure black carbon (BC) band. The principle of aethalometer was to measure the optical attenuation of BC and then retrieve the BC mass concentrations. The outside BC particles were inhaled into the primary chamber of aethalometer through stainless steel. Then the BC particles adhered to the quartz membrane. The absorption attenuation of BC, then, can be obtained according to light exposure [31]. Based on the attenuation of light values, the mass concentration of BC, then, can be calculated continuously [30,32]. The flow rate of the equipment is 5 L·min^{-1} and the sampling frequency is 2 min. We maintained the stability of the light source every day to ensure the accuracy of the data and conduct calibration every three months.

2.2. Methodology

The aerosol scattering coefficient σ_s and the backscattering coefficient β_s are the important aerosol optical parameters and manifest the particle scattering capacity. The σ_s and β_s can be obtained directly from the nephelometer. In this study, we used the 550 nm of σ_s and β_s [2,3]. At the same time, the scattering Ångström index α_s can be calculated based on the σ_s:

$$\alpha_s = -\frac{\ln[\sigma_s 700\ \text{nm}/\sigma_s(450\ \text{nm})]}{\ln(700\ \text{nm}/450\ \text{nm})} \quad (1)$$

α_s reveals the aerosol sizes characteristic according to the Mie theory. The lower the values of α_s, the higher the aerosol size values [23]. The change in α_s is governed by the aerosol size distribution. α_s has little relationship with the aerosol concentration. In this study, α_s can be calculated based on σ_s at 450 nm and 700 nm as Equation (1).

At the same time, the study of g and b is helpful to improve the understanding of aerosol properties during haze. Also, aerosol asymmetry factors b and g can usually be calculated using Equations (2) and (3) [33,34]:

The aerosol asymmetry parameter (g) and the backscatter ratio (b) are also aerosol scattering optical parameters. g reflects the forward scattering capability of particles; b reflects the backscattering capability of aerosols. Investigating g and b can help improve the understanding of aerosol properties during haze periods. g and b can also be calculated based on σ_s and β_s [33,34]:

$$b = \beta_s/\sigma_s \quad (2)$$

$$g = -7.14[b]^3 + 7.14[b]^2 - 3.96[b] + 0.98 \quad (3)$$

In this equation, g denotes the aerosol asymmetry factor, and α_s is the total scattering coefficient obtained by the integrated nephelometer; β_s is the backscattering coefficient obtained by the integrated nephelometer. In theory, the range of g is between −1 and 1 [2]. On the other hand, the aerosol absorption coefficient σ_{ab} is also the basic optical parameter and it shows the absorption capacity of the aerosol. σ_{ab} can be calculated indirectly using the BC concentration [29,30,34]:

$$\sigma_{ab} = \alpha \times [BC] \quad (4)$$

Here [BC] is the black carbon mass concentration at 880 nm, which represents the pure black carbon concentrations and can be obtained directly from the aethalometer. α is the absorption efficiency factor, which can be calculated by 14625/λ [31,32]. λ represents the wavelength. In the study, we utilized the σ_{ab} at 532 nm.

Meanwhile, the aerosol single scattering albedo (SSA) is also an important optical parameter of aerosols. SSA can reflect the particles scattering proportion in the whole extinction effect of aerosols. The SSA can be calculated as the following formula:

$$\mathrm{SSA} = \frac{\sigma_s}{\sigma_{ab} + \sigma_s} \tag{5}$$

The aerosol's direct radiative effects can be sensitively revealed in the change of SSA, and SSA can also convey the relative contribution of scattering and absorption [3]. The SSA of pure BC is only 0.2, which indicates that the scattering capacity of BC is low and the absorption capacity of BC is high. SSA values are mainly related to aerosol ingredients and sizes [35]. In this study, we utilized SSA values at 532 nm. So the σ_s should be corrected to 532 nm based on α_s:

$$\sigma_s(532\ \mathrm{nm}) = \sigma_s(550\ \mathrm{nm}) \times \left[\frac{520\ \mathrm{nm}}{550\ \mathrm{nm}}\right]^{-\alpha_s} \tag{6}$$

In all, the aerosol scattering (σ_s) and absorption (σ_{ab}) coefficients, SSA (ω_0), scattering Ångström exponents (α_s), backscatter ratio (b), and asymmetry factor (g) are the defining parameters that characterize the primary aerosol optical properties, which can help to quantitatively gauge the radiation forcing of aerosols, especially in haze weather. The contribution of each optical parameter during haze and haze-free conditions was of our pertinent interest, which required long-term accumulation experiments. The different characteristics of each aerosol optical parameter in haze and haze-free periods can enable us to have a clearer and more detailed understanding of the aerosol radiation effect on haze (e.g., we can determine which optical parameters change dramatically). On the other hand, according to the varied contributions of aerosol optical properties, discrimination methods of haze and haze-free aerosols can also be developed.

2.3. Support Vector Machine Algorithm

To further explore the contribution of each optical characteristic parameter of haze and haze-free aerosol particles, we selected data from December 2009 to September 2014 (370 days of non-haze and 662 days of haze conditions). In this study, we also utilized the weather datasets provided by the Wuhan Meteorological Bureau [36]. At present, the definition of haze standards is not consistent around the world. For example, the Chinese Meteorological Administration (CMA) decided that if visibility values are less than 10 km and relative humidity (RH) values are less than 95%, it is haze weather. In some studies, researchers reported that if visibility values are less than 5 km and RH values are less than 80%, it defines haze weather [13,14]. Also, it is challenging to link haze-days with aerosol optical properties. Therefore, in this study, we utilized the weather datasets provided by Wuhan Meteorological Bureau, which utilized the criterion that visibility values are less than 5 km and RH values are less than 80% [36]. A support vector machine (SVM) algorithm was employed to calculate the classification accuracy of each optical parameter (Figure 2). The Kolmogorov-Smirnov statistical method was used for testing, and statistical methods were also applied to verify the result. Then, the contribution of each optical parameter under haze and haze-free conditions was obtained. Finally, according to the optical parameters with large contributions (weights), a convenient and simple optical criterion has been defined to distinguish haze and haze-free aerosols, to help us better understand the radiation forcing effect of haze aerosols.

The SVM is a generalized linear classifier that carries out binary classification on data according to supervised learning [37]. The decision boundary of the SVM is the maximum margin hyperplane, which is solved for the learning samples to create a classification hyperplane as a decision surface

to maximize the edge of the isolation between the different classes [38]. The SVM used the hinge loss function to calculate empirical risks and added a regularization term into the solving system to optimize the structural risk, which was a classifier with sparsity and robustness. The SVM can conduct non-linear classification through the kernel method, which is one of the common kernel learning methods. As shown in Figure 2, we first chose the training database to find the support vectors in the hyperplane and then used the trained model for classification. Finally, the classification accuracy of each training parameter was obtained. We can utilize the classification accuracy to decide which parameter has the most significant effect on the classification.

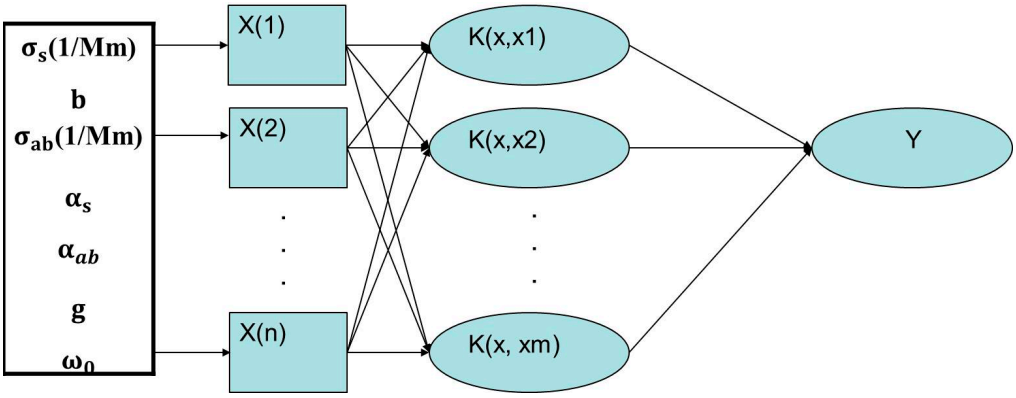

Figure 2. Flow chart of the support vector machine (SVM) in this experiment [37].

3. Results and Discussion

3.1. Overview of Aerosol Scattering and Absorption Properties

Figure 3 depicts the temporal series of daily average aerosol optical properties measured at Wuhan from December 2009 to September 2014. The statistics of the optical parameters based on daily average data including means, standard deviations, percentiles (1, 10, 25, 50, 75, 99 percentiles), and skewness are reported in Table 1. The skewness measures the asymmetry degree of the optical parameters. When the skewness is >0, the frequency distribution is skewed to the right, and vice versa. Normal distributions are symmetrical with skewness of 0. All parameters demonstrate a skewness higher than 1 except SSA (ω_0, −2.59), scattering Ångström exponents (α_s, 0.11) and asymmetry factor (g, −0.93). Negative skewness indicates that values lower than the mean are more probable than values higher than the mean. Similar SSA skewness values have been reported by Pandolfi et al. at the MSY RB site as well as the MSC site [39]. Negative skewness for g is a consequence of the high positive skewness observed for b. As shown in Table 1, both σ_s and σ_{ab} show skewness higher than 1, so we can see that the mean σ_s is 25% larger than its median and σ_{ab} is 38% greater than its median.

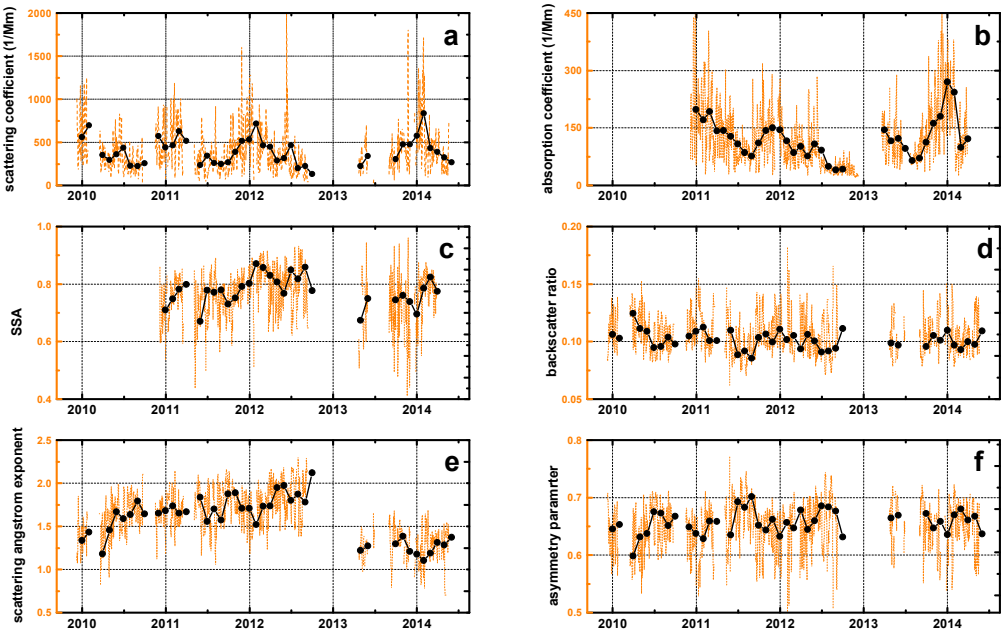

Figure 3. The temporal series of hourly average aerosol optical properties. Black dotted lines represent the monthly mean values. Where (**a**) scattering coefficient (Mm^{-1}), (**b**) absorption coefficient (Mm^{-1}), (**c**) SSA, (**d**) backscatter ratio, (**e**) scattering Ångström index, (**f**) asymmetry parameter.

Significant seasonal variations can be found for all the aerosol optical properties. Strong fluctuations, mainly related to the change of synoptic systems, also appear in all-time series. Large variations for the whole aerosol scattering and absorption coefficients also exist. Hourly aerosol scattering (σ_s) at 550 nm at the LIESMARS site ranged between 12.79 and 1518.65 Mm^{-1}. Mean values of σ_s at 550 nm is 322.54 Mm^{-1}. Aerosol absorption (σ_{ab}) coefficients at 532 nm ranged between 6.92 and 133.66 Mm^{-1}. Mean values of σ_{ab} at 532 nm is 35.06 Mm^{-1}. The 99th percent of σ_s and σ_{ab} are as large as 1518.65 Mm^{-1} and 133.66 Mm^{-1}, respectively. The reason could be that some severe haze episodes occurred during the experimental period in Wuhan. As mentioned in the study of Zhang et al., a most serious haze episode caused by biomass combustion occurred in central China (Wuhan) from 6–14 June 2012 [3]. During this haze event, the mean σ_s and σ_{ab} were approximately 5.3, and 3.4 times higher than that of normal weather, respectively, which explains the observed values of the hourly mean maximum of σ_s and σ_{ab} on 11 June 2012. Compared to other long-period measurements around the world, σ_s and σ_{ab} values are similar to those measured in anthropogenically influenced stations in North China [40]. The mean SSA for the entire period was 0.89 (0.08), which was about 0.08 higher than the value reported by Bergin et al. (2001) [40] for Beijing urban area, and also higher than the value (0.85) in climate modelling simulations for China and India performed by Menon et al. (2002) [41].

Table 1. Aerosol optical properties at LIESMARS site in Wuhan city.

Hourly	λ	Counts	Median	Mean	SD	Skewness	Percentiles				
Base			**(50th perc.)**				**1**	**10**	**25**	**75**	**99**
σ_s (Mm^{-1})	450	9366	341.55	414.67	363.97	2.92	17.53	76.12	175.50	540.15	1818.31
	550	9366	258.23	322.54	299.48	3.07	12.79	54.77	127.90	417.24	1518.65
	700	9366	171.35	226.68	223.79	2.80	9.00	35.65	81.95	291.08	1150.25
b	450	9366	0.11	0.12	0.03	14.04	0.09	0.10	0.10	0.12	0.16
	550	9366	0.12	0.12	0.02	2.23	0.08	0.10	0.10	0.13	0.17
	700	9366	0.15	0.15	0.02	0.47	0.10	0.12	0.13	0.17	0.20
σ_{ab} (Mm^{-1})	532	11537	25.42	35.06	28.03	1.78	6.92	11.18	14.94	45.72	133.66
	450–700	9366	1.49	1.52	0.35	0.11	0.74	1.08	1.28	1.76	2.26
α_s	450–550	9366	1.41	1.39	0.29	−0.28	0.71	0.99	1.21	1.60	2.00
	550–700	9366	1.52	1.62	0.46	0.32	0.74	1.07	1.27	2.04	2.53
	450	9366	0.63	0.62	0.06	−10.51	0.51	0.57	0.60	0.65	0.70
g	550	9366	0.62	0.61	0.05	−0.93	0.49	0.54	0.58	0.65	0.71
	700	9366	0.55	0.55	0.05	−0.01	0.43	0.48	0.51	0.59	0.65
ω_0	532	6607	0.91	0.89	0.08	−2.59	0.52	0.80	0.87	0.93	0.97

Table 1 shows aerosol optical properties at the LIESMARS site in Wuhan city. The mean values of σ_s, σ_{ab}, and SSA are 322.54 Mm^{-1}, 35.06 Mm^{-1}, and 0.89, respectively. The mean σ_s and σ_{ab} of Wuhan (σ_s/σ_{ab}) are considerably lower than that of Beijing (488 Mm^{-1}/83 Mm^{-1}) and Guangzhou (418 Mm^{-1}/91 Mm^{-1}) [40,42]. The σ_s of Wuhan is slightly larger than that in Shanghai (293 Mm^{-1}) while the σ_{ab} is lower than that in Shanghai (65.81 Mm^{-1}) [15]. Wuhan, an intensely industrialized megacity, hosts diverse sources of aerosols. Thus, σ_s and σ_{ab} were reasonably larger than some rural zones, such as SDZ site (174.6 Mm^{-1}/17.5 Mm^{-1}) [43]; coastal sites in western countries, such as BND site (57.0 Mm^{-1}/4.62 Mm^{-1}) in North America [44] and some high altitude sites in the top of the mountain, such as Melpitz site (53.37 Mm^{-1}/ 5.64 Mm^{-1}) in Germany [45]. On average, the absolute values of extensive optical properties and their amplitudes are higher at the LIESMARS site compared with the above-mentioned sites. The urban site is close to anthropogenic pollutant emissions compared to rural and mountain sites and make more effective the pollution potential of thermally driven atmospheric processes such as the PBL oscillations [46]. As a consequence, the Wuhan station showed marked optical properties due to the effectiveness of the emission of highly fine particles of anthropogenic origin in Wuhan. The mean SSA in LIESMARS station (0.89) is about 0.01 larger than the values in the SDZ site (0.88) and it is slightly lower than that in the BND site (0.91). The SSA in Wuhan was remarkably larger than 0.83 in Guangzhou, 0.81 in summer in Beijing, and 0.81 in Shanghai [40,42]. Dubovik et al. [47] calculated the range of SSA (0.85–0.95) for the northern hemisphere using the Aerosol Robotic Network (AERONET) inversion. The results of this study are close to the results of AERONET-based study by Dubovik et al. The mean values of b at 550 nm, scattering Ångström exponents (α_s, 450–700 nm), and g at 550 nm measured at LIESMARS site were 0.12 ± 0.02, 1.52 ± 0.35, 0.61 ± 0.05, respectively. These values were very close to the values reported for the Jungfraujoch site and MSC site [28], indicating similarities in the mean aerosol characteristics observed at these stations. The changes in aerosol α_s, b, and g are related to aerosol composition and age [35].

Figure 4 portrays the correlations between the frequency distribution of aerosol optical and physical properties. Similar relationships were also discussed in the researches of [28,40,44,48]. This kind of relationship can be a benefit to enhance the precision of algorithms for retrieving aerosol properties [44]. As depicted in Figure 4a, aerosol scattering coefficients (σ_s) has an obvious linear positive correlation with aerosol backscattering coefficients (β_s). This phenomenon can easily be understood. When aerosol concentration increases, the total scattering effect gets enhanced, and, hence, the increase in backscattering coefficients. The same results were also observed at MSC site [28], MSY RB site [40] and a similar phenomenon has also been reported at AND2011 [48]. Aerosol scattering coefficients (σ_s) have also a certain positive correlation with aerosol absorption coefficients (σ_{ab}) (Figure 4b), which can be due to the higher concentrations of aerosols, in turn, leading to increased total scattering as well as absorption effects. This observation can also be found in the research of MSC site [28], MSY RB site [40], and AND2011 [48]. Figure 4c reveals the slight rise in aerosol SSA with the increase in aerosol scattering

coefficients (σ_s) for Wuhan city. This indicates that the aerosol scattering effect proportion would slightly increase when aerosol concentrations get enhanced in some haze days in Wuhan [2,35]. In haze days, the aerosol contents were mostly sulfate, nitrate, and organic aerosols, which can also accentuate the proportions of aerosol scattering effects [2,35,40,48,49]. Figure 4d shows that scattering Ångström exponents (α_s) has a certain negative correlation with aerosol scattering coefficients. This indicates that when a haze episode occurs, the aerosol scattering coefficients become higher, and the aerosol sizes also get enhanced, simultaneously [50,51]. Because during haze episodes, aerosol contents are mostly sulfate, nitrate, organic, and secondary aerosol aerosols from a photochemical reaction, which can lead to bigger aerosol sizes [2,3,35,48,49,52,53]. Aerosol asymmetry factor (g) has also an obvious positive correlation with aerosol scattering coefficients (σ_s) (Figure 4e). The reason being, when aerosol concentration is increased, the total scattering effect gets enhanced, and so does the forescattering effects. The same results were observed at the MSC site [28], MSY RB site [40], and a similar phenomenon was reported by AND2011 [48]. According to formula 5, backscatter ratio, hence, has an obvious negative correlation with aerosol scattering coefficients (σ_s) (Figure 4f). This indicates that the aerosol backscattering effects proportion can decrease when aerosol concentrations get enhanced in some haze-episode days in Wuhan. This observation is also in agreement with the MSC site [28].

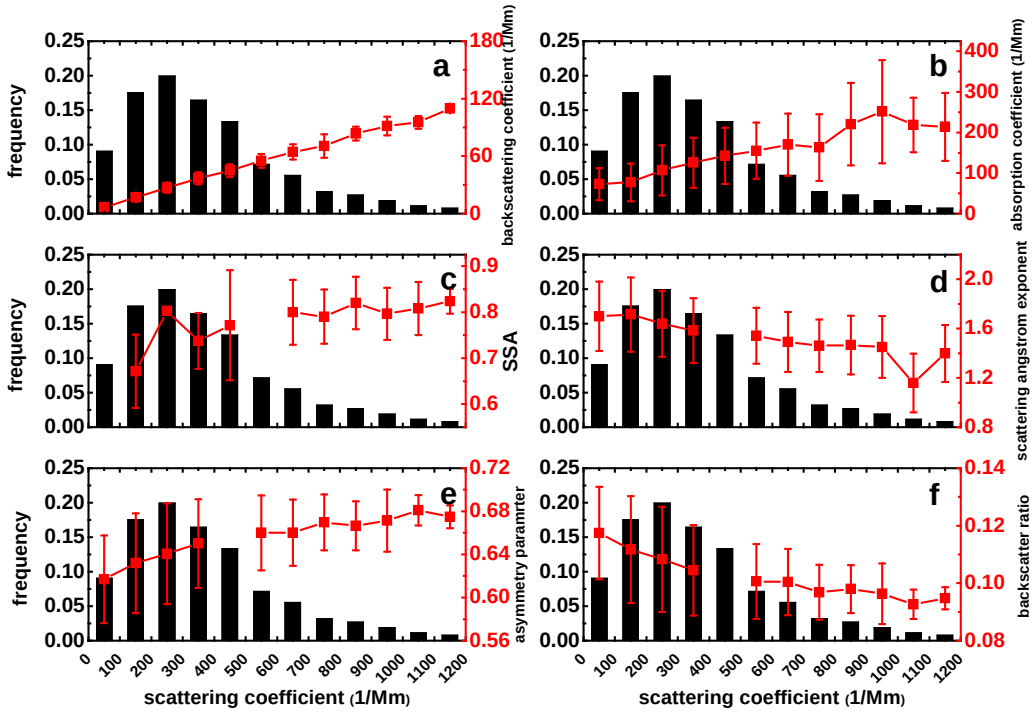

Figure 4. Correlation between the frequency distribution of aerosol scattering coefficients (σ_s) and (**a**) aerosol backscattering coefficients (β_s) at 550 nm; (**b**) absorption coefficients (σ_{ab}) at 550 nm; (**c**) single scattering albedo (SSA) at 550 nm; (**d**) scattering Ångström exponents (α_s) at 550 nm; (**e**) asymmetry factor (g) at 550 nm; (**f**) backscatter ratio (b) at 550 nm.

3.2. Seasonal Variation of Aerosol Scattering and Absorption Properties

The average annual cycles of aerosol optical properties at the LISMARS site are shown in Figure 5. Table 2 lists the average aerosol optical properties in each month. It can be seen in Figure 5 that annual cycles are evident for all aerosol optical properties. The σ_s and σ_{ab} have nearly the same variation pattern, with relatively higher values in winter and lower values in summer. The maximum and minimum of mean monthly σ_s are in January (759.66 Mm^{-1}) and July (129.31 Mm^{-1}), respectively. The maximum and minimum of mean monthly σ_s are in the January (71.00 Mm^{-1}) and August (18.73 Mm^{-1}), respectively. Large variations in the monthly aerosol scattering and absorption levels existed in Wuhan city. The mean monthly values of σ_s and σ_{ab} are always higher than the median

values, especially in winter, indicating that heavier pollution events rather occur in winter than in summer. These findings were the same in the research of Wang et al. [35] and Zhang et al. [2]. A similar phenomenon was also observed at the regional GAW observation site Melpitz in East Germany. The annual cycles of σ_s and σ_{ab} are mainly determined by the annual variation of the boundary layer height [2]. In winter, the local emission is higher due to a larger amount of fossil fuel combustion. The wintertime shallow mixing layer favors the accumulation of aerosol pollutants, thus causing an increase in the level of σ_s and σ_{ab}. In summer, the boundary layer is more unstable because of the surface heating and causes turbulence and vertical mixing, which results in a dilution effect for a pollutant. Therefore, σ_s and σ_{ab} in summer are at a relatively low level and with small variations.

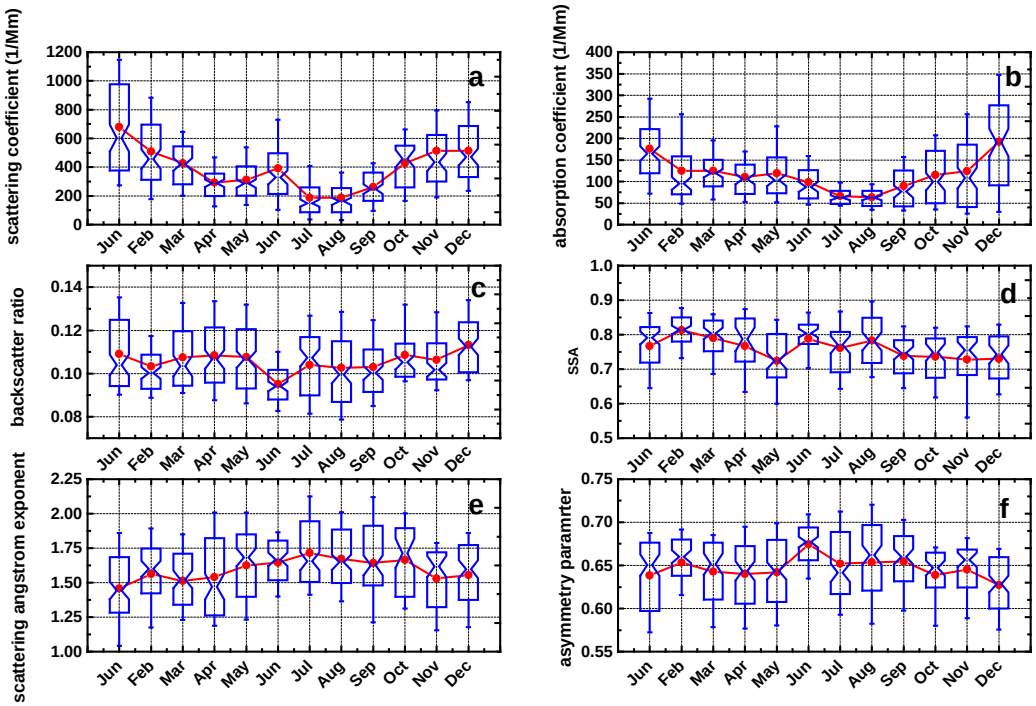

Figure 5. Annual variation curves of aerosol optical properties in the LIESMARS site based on daily means: (**a**) Aerosol scattering coefficients (σ_s) at 550 nm; (**b**) aerosol absorption coefficients (σ_{ab}) at 532 nm; (**c**) backscatter ratio at 550 nm; (**d**) single scattering albedo (SSA) at 532 nm; (**e**) scattering Ångström exponents (α_s); (**f**) asymmetry factor (g) at 550 nm.

The SSA only shows slight annual variations, with high values in summer. This annual pattern might be caused by the variation of regional emission and secondary aerosol formation. In summer, air pollution episodes (such as haze) occur frequently in Wuhan [3]. In these events, secondary aerosol productions via photochemistry processes are efficient and result in a large fraction of non-light-absorbing components such as organic matter and sulfate in a particulate matter [37], hence yielding a relatively higher level of SSA. The evident annual cycle can be found in the backscatter ratio (b), with higher values in winter. This annual pattern can be attributed to the variation of both the number size distribution and the mixing state of particles. A significant nucleation mode can be usually found in the daytime because of the formation of secondary aerosols during hazy weather. According to Collaud Coen et al. (2007) [54], such a decrease in aerosol mean size may increase the b. Also, it was found that the morphology of a black carbon core surrounded by a non-light-absorbing shell would result in a much higher b than the external mixture of the same amount of both components. In winter, because of the active photochemical aging processes, black carbon is close to the morphology of core-shell, thus causes a higher level of b.

Scattering Ångström exponent (α_s) is mainly determined by the shape of the aerosol number size distribution. α_s smaller than 1 indicates that the size distribution is dominated by coarse mode,

whereas α_s larger than 2 indicates that fine mode particles dominate the size distribution [55,56]. The annual pattern of α_s can be explained by the variation of aerosol number size distributions due to secondary particle formation [57,58]. In summer Wuhan, haze episodes often happened owing to straw burning incidents and the atmospheric temperature was also high (Table 2). During such periods, secondary particles can form due to photochemical processes. High concentrations of small particles cause a high level of α_s, thus results in higher average α_s in summer compared to other seasons.

Table 2. Monthly averages and standard deviations of aerosol optical properties at the LIESMARS site.

Parameter	σ_s (Mm^{-1})	σ_b (Mm^{-1})	b	σ_{ab} (Mm^{-1})	α_s	g	ω_0
λ (nm)	550	550	550	532	450–700	550	532
Jan	759.66 (389.39)	88.10 (36.79)	0.12 (0.02)	71.00 (30.16)	1.14 (0.26)	0.60 (0.05)	0.91 (0.03)
Feb	395.70 (261.51)	43.53 (26.48)	0.11 (0.01)	29.26 (19.41)	1.30 (0.31)	0.62 (0.03)	0.93 (0.02)
Mar	360.27 (145.30)	41.98 (14.54)	0.12 (0.01)	38.95 (18.09)	1.32 (0.13)	0.61 (0.03)	0.92 (0.03)
Apr	267.76 (156.21)	31.40 (16.03)	0.12 (0.02)	30.98 (18.70)	1.69 (0.31)	0.60 (0.04)	0.90 (0.07)
May	311.63 (172.27)	34.96 (17.97)	0.12 (0.02)	36.66 (23.54)	1.60 (0.35)	0.62 (0.05)	0.90 (0.04)
Jun	375.12 (495.23)	38.64 (47.67)	0.11 (0.01)	33.40 (21.60)	1.64 (0.20)	0.64 (0.03)	0.94 (0.02)
Jul	129.31 (134.54)	13.87 (11.56)	0.12 (0.02)	20.01 (7.29)	1.72 (0.31)	0.61 (0.05)	0.80 (0.14)
Aug	149.92 (131.50)	16.79 (13.11)	0.12 (0.04)	18.73 (9.09)	1.63 (0.32)	0.61 (0.09)	0.82 (0.15)
Sep	248.67 (158.79)	28.16 (15.51)	0.12 (0.02)	24.76 (16.74)	1.51 (0.40)	0.61 (0.05)	0.89 (0.05)
Oct	444.12 (204.78)	54.27 (22.33)	0.12 (0.01)	31.12 (25.17)	1.41 (0.14)	0.60 (0.03)	0.90 (0.04)
Nov	436.73 (413.83)	52.31 (39.34)	0.13 (0.02)	34.12 (33.36)	1.23 (0.21)	0.58 (0.05)	0.87 (0.05)
Dec	520.70 (175.93)	71.42 (19.44)	0.14 (0.01)	65.97 (40.30)	1.24 (0.18)	0.56 (0.03)	0.88 (0.03)

Standard deviation is in parentheses.

3.3. SVM Results

SVM has been applied to independently classify the optical parameters of haze and haze-free aerosols, to determine the classification accuracy of each parameter. High precision indicates high importance, and low precision indicates low importance. To verify the results rendered by SVM, each parameter has been statistically tested by using the Kolmogorov-Smirnov test. This enabled to identify the important optical parameters to be used as haze aerosol indicators. Further, based on the probability density distribution of the indicator parameters, the classification standards of haze aerosol particles were defined.

We had a total of 370 samples of mean daily values in the haze-free period and 662 samples of mean daily values in haze aerosol conditions; 150 haze-free samples and 300 haze samples were randomly selected as the training datasets. However, the remaining 220 haze-free samples and 362 haze samples were selected as the testing dataset. The classification accuracy of each aerosol optical parameter is presented in Table 3. It can be seen that the aerosol scattering coefficient (σ_s) and absorption coefficient (σ_{ab}) have the highest accuracy (85.37% and 74.53%, respectively), which attest that these are the most important indicators in distinguishing haze and haze-free weather.

To verify the preliminary results of the SVM, we first used statistical analysis. The mean value and standard deviation of each aerosol optical parameter were calculated for both the haze and haze-free days. As can be seen in Table 4, σ_s is 2.89 times higher for haze days (540.21 Mm^{-1}) than for haze-free days (186.96 Mm^{-1}); while the σ_{ab} is 2.03 times higher for haze days (153.27 Mm^{-1}) than for haze-free days (75.34 Mm^{-1}). Other aerosol optical parameters (b, α_s, α_{ab}, g, and ω_o) show no significant differences between haze-free and haze days. Further, the Kolmogorov-Smirnov test was used to examine the distribution differences of each optical parameter in haze and haze-free conditions (Table 5). Compared with other optical parameters, the aerosol scattering coefficient σ_s and absorption coefficient σ_{ab} have very small p values with much lower magnitudes than do the other parameters, indicating significant differences in these values between haze and haze-free days. These results are aligned with the previous SVM results. Therefore, σ_s and σ_{ab} are verified as the main factors to quantitatively distinguish between haze and haze-free conditions.

Table 3. The SVM classification accuracies of every aerosol optical parameter. σ_s is the aerosol scattering coefficient at 550 nm (Mm^{-1}); b is the aerosol backscattering ratio at 550 nm; σ_{ab} is the aerosol absorption coefficient at 520 nm (Mm^{-1}); α_s is the aerosol scattering Ångström exponent at 450–700 nm; α_{ab} is the aerosol absorption Ångström exponent at 370–950 nm; g is the aerosol asymmetry factor at 550 nm; and ω_0 is the aerosol single scattering albedo at 550 nm.

Parameters	Training (Haze-Free/Haze)	Testing (Haze-Free/Haze)	Accuracy
σ_s	150/300	220/362	85.37%
b	150/300	220/362	69.02%
σ_{ab}	150/300	220/362	74.53%
α_s	150/300	220/362	72.46%
α_{ab}	150/300	220/362	62.13%
g	150/300	220/362	62.13%
ω_o	150/300	220/362	67.81%
All	150/300	220/362	66.95%

Table 4. Statistics of each aerosol optical parameter on haze and haze-free days.

	Haze		Haze-Free	
	Mean	**SD**	**Mean**	**SD**
σ_s	540.21	283.70	186.96	89.36
b	0.10	0.02	0.12	0.02
σ_{ab}	153.27	76.66	75.34	32.32
α_s	1.72	0.19	1.92	0.22
α_{ab}	1.09	0.17	1.04	0.22
g	0.65	0.04	0.61	0.05
ω_o	0.78	0.06	0.71	0.07

Table 5. The results of the Kolmogorov-Smirnov test each aerosol optical parameter.

P	σ_s	b	σ_{ab}	α_s	α_{ab}	g	ω_o
σ_s	2.35×10^{-39}						
b		1.44×10^{-11}					
σ_{ab}			6.55×10^{-17}				
α_s				6.54×10^{-10}			
α_{ab}					1.28×10^{-4}		
g						1.44×10^{-11}	
ω_o							1.09×10^{-11}

Given these results, the next step was to quantitatively determine the discrimination criteria based on the two indicator factors in Wuhan City. Figure 6 depicts the relationship between σ_s and σ_{ab} for haze-free (Figure 6a) and haze (Figure 6b) aerosols. For haze-free aerosols, the main range of σ_s is 50–300 Mm^{-1}, while for haze days, there is a wider range of 250–1700 Mm^{-1}. The σ_s values have almost no overlapping ranges for haze and haze-free days, which indicated that σ_s has an obvious distinction between haze and haze-free aerosols, indicating that the σ_sSVM classification accuracy is the highest (Table 3). At the same time, the main range of σ_{ab} is 30–100 Mm^{-1} for haze-free days and 50–150 Mm^{-1} for haze days. σ_{ab} demonstrates some overlap between haze and haze-free days; therefore, the σ_{ab}SVM classification accuracy is lower than that of σ_s (Table 3). This might be because the local absorbing aerosol concentrations (mainly black carbon aerosols) did not change much between haze and non-haze periods, while the scattering aerosol concentrations (mainly sulfate and nitrate aerosols) changed greatly.

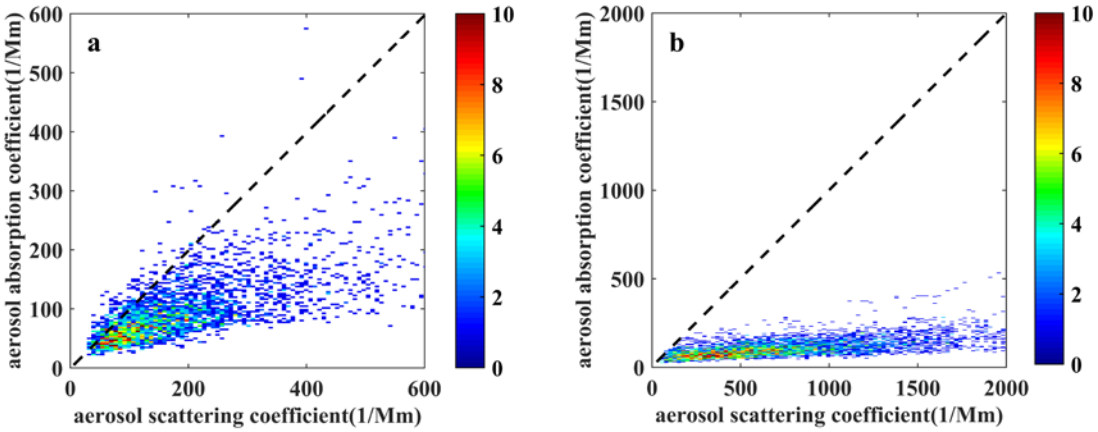

Figure 6. Relationship between aerosol scattering coefficients and absorption coefficients: (**a**) haze-free aerosols; (**b**) haze aerosols. The scatter points represent the number of days. The red solid circles represent high-frequency distributions. The dashed line represents the 1:1 line.

The σ_s and σ_{ab} distributions of haze and haze-free aerosols exhibit a marked difference that can be used to distinguish between them. According to the distribution differences of σ_s and σ_{ab} between haze and haze-free aerosols, a quantitative criterion can be established to distinguish haze and haze aerosols. To devise such quantitative criteria, the frequency histograms of the aerosol scattering (σ_s) and absorption coefficients (σ_{ab}) are displayed in Figure 7. As shown, the peak of σ_s was approximately 150 and 450 Mm^{-1} for the haze-free and haze days, respectively, and the intersection of the σ_s frequency distribution of haze-free and haze was 250 Mm^{-1} (Figure 7a). Thus, a threshold of 250 Mm^{-1} for σ_s could be used to distinguish between haze and haze-free conditions. Similarly, the peak σ_{ab} values are approximately 75 and 150 Mm^{-1} for haze-free and haze days, respectively, and the intersection of the σ_s frequency distribution of haze-free and haze conditions is 75 Mm^{-1} (Figure 7b). Thus, a threshold of 75 Mm^{-1} for σ_{ab} could be used to further distinguish between the two weather conditions.

In conclusion, the σ_s and σ_{ab} thresholds can be combined to identify haze aerosols.

(1) For $\sigma_s > 250$ Mm^{-1} and $\sigma_{ab} > 75$ Mm^{-1}, the aerosols are identified as haze aerosols.
(2) For $\sigma_s < 250$ Mm^{-1} but $\sigma_{ab} > 75$ Mm^{-1}, the aerosols are also identified as haze aerosols.
(3) For $\sigma_{ab} < 75$ Mm^{-1} but $\sigma_s > 250$ Mm^{-1}, the aerosols are also identified as haze aerosols.
(4) For $\sigma_s < 250$ Mm^{-1} and $\sigma_{ab} < 75$ Mm^{-1}, the aerosols are identified as haze-free aerosols. We used this new standard to identify haze aerosols from our database, and the detection accuracy was 81.49%, indicating that the standard was suitable to distinguish between haze and haze-free aerosols in Wuhan City.

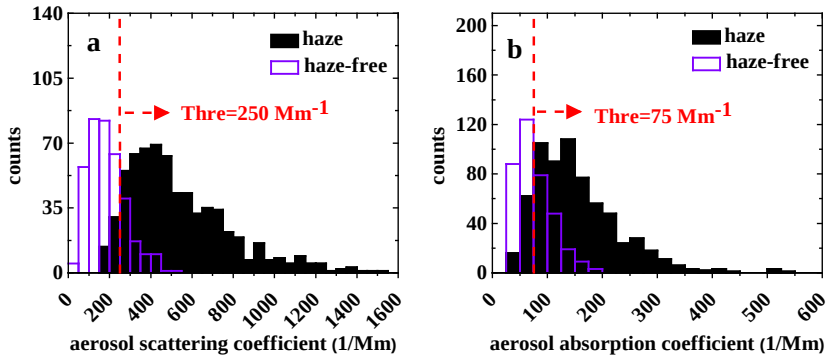

Figure 7. Haze-free (purple histogram) and haze (black column) frequency histograms of aerosol scattering (σ_s) (**a**) and absorption coefficients (σ_{ab}) (**b**). The red dashed line represents the thresholds for distinguishing between haze and non-haze aerosols.

4. Conclusions

Based on the experimental datasets for four years, the weighted contributions of various aerosol optical parameters of haze and haze-free conditions have been quantitatively studied. The SVM algorithm was used to classify each optical parameter independently, and the indicator factor with the greatest influence was statistically determined by its classification precision. The results reveal that the aerosol scattering coefficient σ_s (85.37%) and absorption coefficient σ_{ab} (74.53%) have the highest classification accuracy levels. To verify the SVM results, a Kolmogorov-Smirnov statistical test and traditional statistical analysis were utilized. Results demonstrate that both σ_s and σ_{ab} have small p values, indicating that their frequency distributions differed greatly between haze and non-haze aerosols. Meanwhile, the σ_s values during haze are 2.89 times that during haze-free weather, and the σ_{ab} values during haze are 2.03 times that during haze-free weather. Based on the differences in the σ_s and σ_{ab} probability distributions between haze and haze-free aerosols, a quantitative criterion has been proposed to distinguish between haze and haze-free aerosols. After testing, the accuracy rate of this standard is 81.49%. This detailed study on the optical properties of haze aerosols can provide a scientific basis for local environmental departments to formulate atmospheric governance policies.

Overall, this study provides a better understanding of air pollution in the YERB region. In the future study, aerosol types and their microphysical properties over the region will be considered. Also, the vertical feature mask (VFM) products of CALIPSO will be considered to investigate the vertical structure and layers stratification characteristic of different aerosol species.

Author Contributions: Conceptualization, M.Z.; methodology, M.Z., and C.Z.; software, C.Z. and J.L.; validation, G.H., and W.G.; investigation, M.Z.; writing—original draft preparation, M.Z.; writing—review and editing, M.B., M.N., and L.A.; project administration, M.Z.; funding acquisition, M.Z. All authors have read and agreed to the published version of the manuscript.

Funding: This research was funded by the National Natural Science Foundation of China (No. 41801282), Programs for Science and Technology Development of Henan Province (No. 192102310008), the Key Scientific Research Project of Henan Institutions of Higher Learning (No. 18B170007), Nanyang Normal University Scientific Research Project (No. ZX2017014), the Science and Technology Project of Nanyang City (No. 2017JCQY017), and the Special Project of Jiangsu Distinguished Professor (1421061801003 and 1421061901001).

Acknowledgments: We would also like to thank the editors for modifying and revising this manuscript.

Conflicts of Interest: The authors declare no conflict of interest.

References

1. Hinds, W.C. Aerosol technology. *Wiley Sons* **2000**, *31*, 175.
2. Gong, W.; Zhang, M.; Han, G.; Ma, X.; Zhu, Z. An investigation of aerosol scattering and absorption properties in wuhan, central china. *Atmosphere* **2015**, *6*, 503–520. [CrossRef]
3. Zhang, M.; Ma, Y.; Gong, W.; Zhu, Z. Aerosol optical properties of a haze episode in wuhan based on ground-based and satellite observations. *Atmosphere* **2014**, *5*, 699–719. [CrossRef]
4. Zhang, M.; Wang, L.; Bilal, M.; Gong, W.; Zhang, Z.; Guo, G. The characteristics of the aerosol optical depth within the lowest aerosol layer over the tibetan plateau from 2007 to 2014. *Remote Sens.* **2018**, *10*, 696. [CrossRef]
5. Markku, K.; Jenni, K.; Heikki, J.; Katrianne, L.; Manninen, H.E.; Tuomo, N.; Tuukka, P.J.; Mikko, S.; Siegfried, S.; Pekka, R. Direct observations of atmospheric aerosol nucleation. *Science* **2013**, *339*, 943–946.
6. Mcmurry, P.H. A review of atmospheric aerosol measurements. *Atmos. Environ.* **2000**, *34*, 1959–1999. [CrossRef]
7. Magistrale, P.V. *Health Aspects of Air Pollution*; Springer: Berlin/Heidelberg, Germany, 1992; pp. 25–31.
8. Tie, X.; Wu, D.; Brasseur, G. Lung cancer mortality and exposure to atmospheric aerosol particles inguangzhou, china. *Atmos. Environ.* **2009**, *43*, 2375–2377. [CrossRef]
9. Edenhofer, O. *Climate Change 2014: Mitigation of Climate Change: Working Group III Contribution to the Fifth Assessment Report of the Intergovernmental Panel on Climate Change*; Cambridge University Press: Cambridge, UK, 2014.

10. Rosenfeld, D. Suppression of rain and snow by urban and industrial air pollution. *Int. J. Food Microbiol.* **2000**, *287*, 40–50. [CrossRef] [PubMed]
11. Twomey, S. The influence of pollution on the shortwave albedo of clouds. *J. Atmos. Sci.* **1977**, *34*, 1149–1154. [CrossRef]
12. Parrish, D.D.; Tong, Z. Climate change. Clean air for megacities. *Science* **2009**, *326*, 674–675. [CrossRef]
13. Vautard, R.; Yiou, P.; Oldenborgh, G.J.V. Decline of fog, mist and haze in europe over the past 30 years. *Nat. Geosci.* **2009**, *2*, 115–119. [CrossRef]
14. Quan, J.; Zhang, Q.; He, H.; Liu, J.; Huang, M.; Jin, H. Analysis of the formation of fog and haze in north china plain (ncp). *Atmos. Chem. Phys.* **2011**, *11*, 8205–8214. [CrossRef]
15. Xu, J.; Tao, J.; Zhang, R.; Cheng, T.; Leng, C.; Chen, J.; Huang, G.; Li, X.; Zhu, Z. Measurements of surface aerosol optical properties in winter of shanghai. *Atmos. Res.* **2012**, *109–110*, 25–35. [CrossRef]
16. Lijie, H.; Lunche, W.; Aiwen, L.; Ming, Z.; Xiangao, X.; Minghui, T.; Hao, Z. What drives changes in aerosol properties over the Yangtze River basin in past four decades? *Atmos. Environ.* **2018**, *190*, 269–283.
17. Shen, X.L.; Dang, T.G.; Liu, J. Summary of beijing-tianjin-hebei haze causes and solutions research. *Adv. Mater. Res.* **2014**, *1010–1012*, 639–644. [CrossRef]
18. Tao, M.; Chen, L.; Lin, S.; Tao, J. Satellite observation of regional haze pollution over the north china plain. *J. Geophys. Res. Atmos.* **2012**, *117*. [CrossRef]
19. Huang, J.; Zhang, W.; Zuo, J.; Jianrong, B.I.; Shi, J.; Wang, X.; Chang, Z.; Huang, Z.; Yang, S.; Zhang, S. An overview of the semi-arid climate and environment research observatory over the loess plateau. *Adv. Atmos. Sci.* **2008**, *25*, 906. [CrossRef]
20. Yan, W.; Che, H.; Ma, J.; Qiang, W.; Shi, G.; Chen, H.; Goloub, P.; Hao, X. Aerosol radiative forcing under clear, hazy, foggy, and dusty weather conditions over Beijing, China. *Geophys. Res. Lett.* **2009**, *36*, 150–164.
21. Ramanathan, V.; Chung, C.; Kim, D.; Bettge, T.; Buja, L.; Kiehl, J.T.; Washington, W.M.; Fu, Q.; Sikka, D.R.; Wild, M. Atmospheric brown clouds: Impacts on south Asian climate and hydrological cycle. *Proc. Natl. Acad. Sci. USA* **2005**, *102*, 5326–5333. [CrossRef]
22. Xia, X.; Chen, H.B.; Wang, P.C.; Zhang, W.X.; Holben, B.N. Variation of column-integrated aerosol properties in a Chinese urban region. *J. Geophys. Res. Atmos.* **2006**, *111*. [CrossRef]
23. Zhao, X.; Zhang, X.; Pu, W.; Meng, W.; Xu, X. Scattering properties of the atmospheric aerosol in Beijing, China. *Atmos. Res.* **2011**, *101*, 799–808. [CrossRef]
24. Yao, H.; Song, Y.; Liu, M.; Archernicholls, S.; Lowe, D.; Mcfiggans, G.; Xu, T.; Du, P.; Li, J.; Wu, Y. Direct radiative effect of carbonaceous aerosols from crop residue burning during the summer harvest season in east china. *Atmos. Chem. Phys.* **2017**, *17*, 1–39. [CrossRef]
25. Rosenfeld, D. Trmm observed first direct evidence of smoke from forest fires inhibiting rainfall. *Geophys. Res. Lett.* **1999**, *26*, 3105–3108. [CrossRef]
26. Winker, D.M.; Tackett, J.L.; Getzewich, B.J.; Liu, Z.; Vaughan, M.A.; Rogers, R.R. The global 3-d distribution of tropospheric aerosols as characterized by caliop. *Atmos. Chem. Phys.* **2013**, *13*, 3345–3361. [CrossRef]
27. Winker, D.M.; Hunt, W.H.; Mcgill, M.J. Initial performance assessment of caliop. *Geophys. Res. Lett.* **2007**, *34*, 228–262. [CrossRef]
28. Pandolfi, M.; Ripoll, A.; Querol, X.; Alastuey, A. Climatology of aerosol optical properties and black carbon mass absorption cross section at a remote high-altitude site in the western mediterranean basin. *Geophys. Res. Lett.* **2014**, *14*, 6443–6460.
29. Weingartner, E.; Saathoff, H.; Schnaiter, M.; Streit, N.; Bitnar, B.; Baltensperger, U. Absorption of light by soot particles: Determination of the absorption coefficient by means of aethalometers. *J. Aerosol Sci.* **2003**, *34*, 1445–1463. [CrossRef]
30. Bodhaine, B.A. Aerosol absorption measurements at barrow, mauna loa, and the south pole. *J. Geophys. Res.* **1995**, *100*, 8967–8975. [CrossRef]
31. Arnott, W.P.; Hamasha, K.; Moosmüller, H.; Sheridan, P.J.; Ogren, J.A. Towards aerosol light-absorption measurements with a 7-wavelength aethalometer: Evaluation with a photoacoustic instrument and 3-wavelength nephelometer. *Aerosol Sci. Technol.* **2005**, *39*, 17–29. [CrossRef]
32. Lyamani, H.; Olmo, F.J.; Alados-Arboledas, L. Light scattering and absorption properties of aerosol particles in the urban environment of Granada, Spain. *Atmos. Environ.* **2008**, *42*, 2630–2642. [CrossRef]

33. Ma, N.; Birmili, W.; Müller, T.; Tuch, T.; Cheng, Y.F.; Xu, W.Y.; Zhao, C.S.; Wiedensohler, A. Tropospheric aerosol scattering and absorption over central Europe: A closure study for the dry particle state. *Atmos. Chem. Phys.* **2013**, *13*, 27811–27854. [CrossRef]
34. Pandolfi, M.; Ripoll, A.; Querol, X.; Alastuey, A. Climatology of aerosol optical properties and black carbon mass absorption cross section at a remote high-altitude site in the western Mediterranean basin. *Atmos. Chem. Phys.* **2014**, *14*, 3777–3814. [CrossRef]
35. Wang, L.; Gong, W.; Xia, X.; Zhu, J.; Li, J.; Zhu, Z. Long-term observations of aerosol optical properties at Wuhan, an urban site in central China. *Atmos. Environ.* **2015**, *101*, 94–102. [CrossRef]
36. Zhang, X.; Huang, Y.; Zhu, W.; Rao, R. Aerosol characteristics during summer haze episodes from different source regions over the coast city of North China Plain. *J. Quant. Spectrosc. Radiat. Transf.* **2013**, *122*, 180–193. [CrossRef]
37. Cherkassky, V. *The Nature of Statistical Learning Theory*; Springer Science & Business Media: Berlin/Heidelberg, Germany, 1995.
38. Cortes, C.; Vapnik, V. Support-vector networks. *Mach. Learn.* **1995**, *20*, 273–297. [CrossRef]
39. Pandolfi, M.; Cusack, M.; Alastuey, A.; Querol, X. Variability of aerosol optical properties in the western Mediterranean basin. *Atmos. Chem. Phys.* **2011**, *11*, 8189–8203. [CrossRef]
40. Bergin, M.H.; Cass, G.R.; Xu, J.; Fang, C.; Zeng, L.M.; Yu, T.; Salmon, L.G.; Kiang, C.S.; Tang, X.Y.; Zhang, Y.H. Aerosol radiative, physical, and chemical properties in Beijing during june 1999. *J. Geophys. Res.* **2001**, *106*, 17969–17980. [CrossRef]
41. Menon, S.; Hansen, J.; Nazarenko, L.; Luo, Y. Climate effects of black carbon aerosols in china and India. *Science* **2002**, *297*, 2250–2253. [CrossRef]
42. Andreae, M.O.; Schmid, O.; Yang, H.; Chand, D.; Yu, J.Z.; Zeng, L.-M.; Zhang, Y.-H. Optical properties and chemical composition of the atmospheric aerosol in urban Guangzhou, china. *Atmos. Environ.* **2008**, *42*, 6335–6350. [CrossRef]
43. Yan, P.T.; Huang, J.; Mao, J.T.; Zhou, X.J.; Liu, Q.; Zhou, H.G. The measurement of aerosol optical properties at a rural site in northern china. *Atmos. Chem. Phys.* **2008**, *8*, 2229–2242. [CrossRef]
44. Delene, D.J.; Ogren, J.A. Variability of aerosol optical properties at four North American surface monitoring sites. *J. Atmos. Sci.* **2002**, *59*, 1135–1150. [CrossRef]
45. Ma, N.; Birmili, W.; Müller, T.; Tuch, T.; Cheng, Y.F.; Xu, W.Y.; Zhao, C.S.; Wiedensohler, A. Tropospheric aerosol scattering and absorption over central Europe: A closure study for the dry particle state. *Atmos. Chem. Phys.* **2014**, *14*, 6241–6259. [CrossRef]
46. Liu, B.; Ma, Y.; Gong, W.; Zhang, M.; Yang, J. Study of continuous air pollution in winter over Wuhan based on ground-based and satellite observations. *Atmos. Pollut. Res.* **2018**, *9*, 156–165. [CrossRef]
47. Dubovik, O.; Smirnov, A.; Holben, B.N.; King, M.D.; Kaufman, Y.J.; Eck, T.F.; Slutsker, I. Accuracy assessments of aerosol optical properties retrieved from aerosol robotic network (aeronet) sun and sky radiance measurements. *J. Geophys. Res. Atmos.* **2000**, *105*, 9791–9806. [CrossRef]
48. Andrews, E.; Ogren, J.A.; Bonasoni, P.; Marinoni, A.; Sheridan, P. Climatology of aerosol radiative properties in the free troposphere. *Atmos. Res.* **2012**, *102*, 365–393. [CrossRef]
49. Wang, Y.S.; Yao, L.; Wang, L.L.; Liu, Z.R.; Ji, D.S.; Tang, G.Q.; Zhang, J.; Hu, B.; Xin, J.Y. Mechanism for the formation of the January 2013 heavy haze pollution episode over central and eastern China. *Sci. China Earth Sci.* **2014**, *57*, 14–15. [CrossRef]
50. Hand, J.L.; Schichtel, B.A.; Pitchford, M.; Malm, W.C.; Frank, N.H. Seasonal composition of remote and urban fine particulate matter in the united states. *J. Geophys. Res. Atmos.* **2012**, 117. [CrossRef]
51. Pitchford, M.L.; Poirot, R.L.; Schichtel, B.A.; Malm, W.C. Characterization of the winter Midwestern particulate nitrate bulge. *Air Repair* **2009**, *59*, 1061–1069. [CrossRef]
52. Bilal, M.; Nichol, J.E.; Bleiweiss, M.P.; Dubois, D.; Rse, J. A simplified high resolution modis aerosol retrieval algorithm (Sara) for use over mixed surfaces. *Remote Sens. Environ.* **2013**, *136*, 135–145. [CrossRef]
53. Pitchford, M.L.; Malm, W.C. Development and applications of a standard visual index. *Atmos. Environ.* **1994**, *28*, 1049–1054. [CrossRef]
54. Coen, M.C.; Weingartner, E.; Nyeki, S.; Cozic, J.; Henning, S.; Verheggen, B.; Gehrig, R.; Baltensperger, U. Long-term trend analysis of aerosol variables at the high-alpine site jungfraujoch. *J. Geophys. Res. Atmos.* **2007**, *112*. [CrossRef]

55. Eck, T.F.; Holben, B.N.; Reid, J.S.; Dubovik, O.; Smirnov, A.; O'Neill, N.T.; Slutsker, I.; Kinne, S. Wavelength dependence of the optical depth of biomass burning, urban, and desert dust aerosols. *J. Geophys. Res. Atmos.* **1999**, *104*, 31333–31349. [CrossRef]
56. Westphal, D.L.; Toon, O.B. Simulations of microphysical, radiative, and dynamical processes in a continental-scale forest fire smoke plume. *J. Geophys. Res. Atmos.* **1991**, *96*, 22379–22400. [CrossRef]
57. Malm, W.C.; Pitchford, M.L. Comparison of calculated sulfate scattering efficiencies as estimated from size-resolved particle measurements at three national locations. *Atmos. Environ.* **1997**, *31*, 1315–1325. [CrossRef]
58. Larson, L.J.; Largent, A.; Tao, F.-M. Structure of the sulfuric acid? Ammonia system and the effect of water molecules in the gas phase. *J. Phys. Chem. A* **1999**, *103*, 6786–6792. [CrossRef]